Journal of Fluid Science and Technology

Vol. 4, No. 3, 2009

Development of a Simple Impulse Turbine for Nano Hydropower*

Yuji NAKANISHI**, Shouichiro IIO***, Yoji TAKAHASHI**, Akito KATO*** and Toshihiko IKEDA***

**Department of Mechanical Engineering, Kanagawa University,
3-27-1 Rokkakubashi, Kanagawa-ku, Yokohama 221-8686, Japan.
***Department of Environmental Science and Technology, Shinshu University,
4-17-1 Wakasato, Nagano 380-8553, Japan.
E-mail: nakanishi@mech.kanagawa-u.ac.jp

Abstract

The aim of this work is to provide an impulse type hydraulic turbine to utilize unexploited water resources as nano hydropower in the mountainous area. The turbine is simplified to make cheap energy and uses inexpensive components for widespread utilization. The turbine model is tested experimentally to reveal the power characteristics. The flow visualization and numerical simulation are conducted to clarify the behavior of free surface flow in the runner with different nozzle positions. The experimental results show that the maximum runner efficiency of the prototype turbine is 0.56. Numerical simulation shows that the output power depends on the nozzle positions with the impingement of the tail of the jet portion to the backside of the blade. This study gives the fundamental information of the turbine performance to acquire a guideline for future practical applications.

Key words: Nano Hydropower, Impulse Turbine, Performance, Flow Visualization, Particle Method

1. Introduction

Environmental issues as typified by global warming become great concern in recent years. It is obvious that achieving sustainable energy means using natural energy effectively. The hydropower should occupy the attention of electric power generating systems as it is clean and renewable energy sources with highest density, in cooperation with wind and the solar powers. Small/micro/nano hydropower has attracted much attention for recent years mainly because of decrease of construction place for large-scale plants and environmental conservation [(1)-(6)]. The aim of this investigation is to develop a hydraulic turbine to utilize unexploited water resources as nano hydropower, for local production for local consumption. This turbine is suitable for the mountainous area in which the effective flow rate is not sufficient while the head is enough.

For power generation using an extremely small water power of less than 1kW, which is our target, it is difficult to use Pelton turbines that we easily hit on due to a problem in the manufacturing cost. So in this study we propose a newly designed turbine with the simplest components of the minimum requirements to realize impulse water turbines that can be easily manufactured and installed on the places where they are necessary in mountain areas. Our aim here is to evaluate the performance of this simple impulse turbine experimentally and numerically to acquire a guideline for future practical applications.

*Received 4 June, 2009 (No. 09-0245)
[DOI: 10.1299/jfst.4.567]

Nomenclature

A : area of nozzle exit ($= \pi d^2/4$) [m^2]
B : runner width [m] (Fig. 2)
d : nozzle exit diameter [m]
D_1 : jet pitch circle diameter [m] (Fig. 3)
D_B : chord of blade [m] (Fig. 2)
D_R : diameter of runner [m] (Fig. 2)
L : power output from blade [W]
L_w : power of water jet ($=^1/_2\rho A V_j^3$) [W]
N_T : rotational speed of runner [min^{-1}]
P : power output from runner ($=T\omega$) [W]
Q : volume flow rate of water [m^3/s]
T : torque experienced by runner [N・m]
V_j : water jet velocity ($= Q/A$) [m/s]
U_t : runner tip speed ($= \pi D_R N_T/60$) [m/s]
ΔZ : nozzle offset distance [m]
α : rotation angle of blade [deg.]
$\Delta\alpha$: rotation angle of blade after contact with jet [deg.]
η : runner efficiency ($= P/L_w$) [-]
λ : tip speed ratio ($= U_t/V_j$) [-]
θ : nozzle angle [deg.] (Fig. 1)
ρ : water density [kg/m^3]
ω : angular velocity of runner ($=2\pi N_T/60$) [rad/s]

2. Experimental apparatus and procedure

A schematic of test model orientation, instrumentation and measurement system is shown in Fig. 1. The test runner consists of 12 blades and 2 endplates. The runner was mounted on a 10.0 mm diameter stainless steel shaft. The runner shaft is supported directly by the transparent acrylic turbine housing which allows the water behavior to be easily observed. One end of the runner shaft is directly coupled to torque meter and load (powder brake). The measurement of power characteristic was started from unloaded state at the supply voltage of 0V to the powder brake and increasing the load in small steps until the runner stopped. Water is supplied to the nozzle by an electric pump (EBARA, 40FQN6.75C) and piping. After striking the blades, water exit the runner housing through a hole at the base and flows back to an enclosure in which the intake of the pump is located. The volume flow rate of water is measured and controlled using an electromagnetic flowmeter (TOSHIBA, LF410/LF400) and hand-operated valve.

The runner configuration is shown in Fig. 2. The blades and endplates were made of transparent Plexiglas. We chose arc-shaped blades that could be made by using part of a pipe, taking account of the cost in practical application. The blades, which were circular, contained a full 180 deg arc with chord of D_B=0.044 m and width of B=0.03 m. The coordinate system is chosen in such a manner that the origin is located at the center of the runner shaft, the X-axis is the horizontal direction and the Z-axis is the vertical direction. A tilt angle of the jet nozzle is defined as θ by which the horizontal jet is given as θ=0°. The offset distance of the jet nozzle ΔZ is defined as the elevation of the intersection of the jet axis and the z-axis measured from the center of a blade that comes at the top of the runner as shown in Fig.1. The diameter of the nozzle exit is d = 11mm. The flow rate, Q, is set to 1.0×10^{-3} m^3/s and the corresponding jet velocity is V_j=10.52 m/s (or the head of 5.64m).

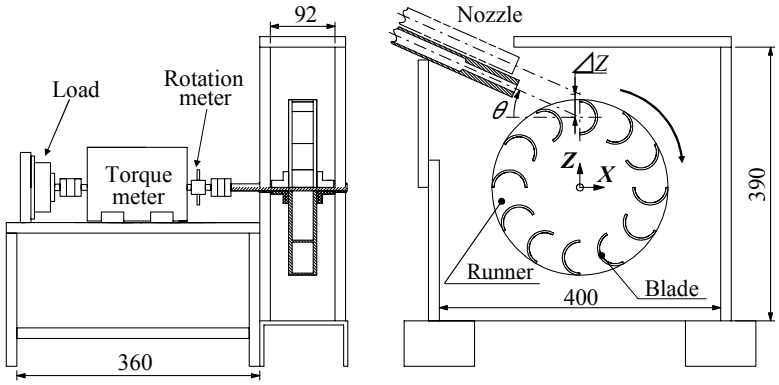

Fig. 1 Experimental apparatus

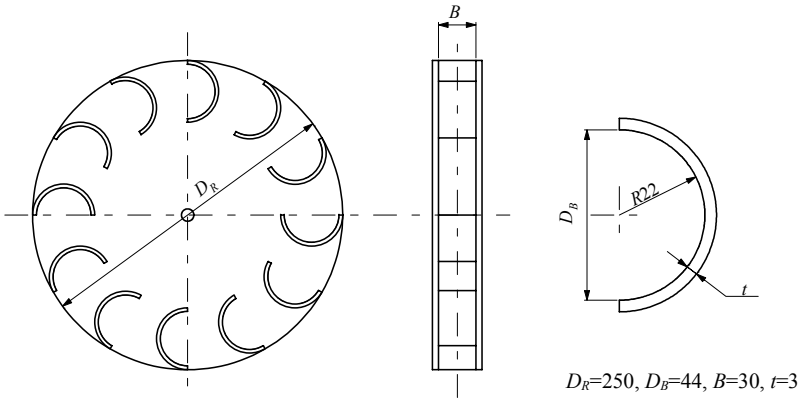

Fig. 2 Model runner

3. Numerical method

In general, numerical simulations of flows in impulse turbines have not been conducted so often compared with reaction turbines since complex free surface flows in rotating runners have to be analyzed. The numerical code based on one of mesh-free particle methods, a Moving-Particle Semi-implicit (MPS) Method[7] enables us to investigate the flow in this impulse turbine. This code has been applied to the simulation of the flow in a Pelton turbine [8,9] making use of its advantages for analysis of free surface flows so far. In the calculation based on the MPS method for incompressible flow, the continuity equation and the Navier-Stokes equation are given as follows:

$$\frac{\partial \rho}{\partial t} = 0 \tag{1}$$

$$\frac{D\boldsymbol{u}}{Dt} = -\frac{1}{\rho}\nabla p + \nu\nabla^2\boldsymbol{u} + \boldsymbol{g} \tag{2}$$

where, ρ, $\boldsymbol{u}$, p, ν and $\boldsymbol{g}$ denote fluid density, velocity vector, pressure, kinematic viscosity and gravitational acceleration, respectively.

In the MPS method, particles are introduced to represent a fluid. Eq. (1) is satisfied by

keeping the particle number density N of each particle constant N_0. The particle number density N_0 is corresponding to the fluid density. The particle number density is defined by summation of a weight w for each particle and considered to be in proportion to the fluid density. The weight w is a function of the distance r between two particles as $w = r_e/r-1$ if $r \leq r_e$, and $w = 0$ if $r > r_e$, where r_e is called as a kernel size.

Gradient and Laplacian operators in Eq. (2) for i-th particle are discretized by the particle interaction models given by Eqs.(3) and (4), respectively.

$$\langle \nabla \phi \rangle_i = \frac{d}{N_0} \sum_{j \neq i} \left[\frac{\phi_j - \phi_i}{|\boldsymbol{r}_j - \boldsymbol{r}_i|^2} (\boldsymbol{r}_j - \boldsymbol{r}_i) \cdot w(|\boldsymbol{r}_j - \boldsymbol{r}_i|) \right] \tag{3}$$

$$\langle \nabla^2 \phi \rangle_i = \frac{2d}{N_0 \lambda_w} \sum_{j \neq i} \left[(\phi_j - \phi_i) \cdot w(|\boldsymbol{r}_j - \boldsymbol{r}_i|) \right], \quad \lambda_w = \frac{\int_V w(r) r^2 dv}{\int_V w(r) dv} \tag{4}$$

where, d is the number of space dimensions. The following Poisson equation of pressure is solved, and then the velocity and position of each particle are corrected so as to obtain the constant particle number density.

$$\langle \nabla^2 p \rangle_i = -\frac{\rho}{\Delta t^2} \frac{\langle N^* \rangle_i - N_0}{N_0} \tag{5}$$

where, $\langle N^* \rangle_i$ is the particle number density at the i-th particle calculated from temporal particle positions updated by Eq. (2) without pressure gradient term. Δt denotes a time step of calculation.

The atmospheric pressure is imposed on particles to represent a free surface and fragmented water, if the condition $N < \beta N_0$ is satisfied. A solid wall is also represented by the same particles as the fluid. The particles of the wall also contribute to the calculation of the particle number density. The particles of the blade and endplate surfaces facing the jet are used for the pressure calculation mentioned above.

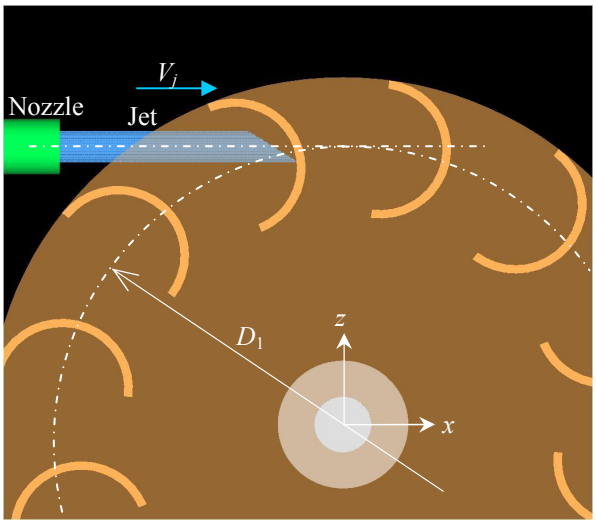

Fig. 3 Jet and runner

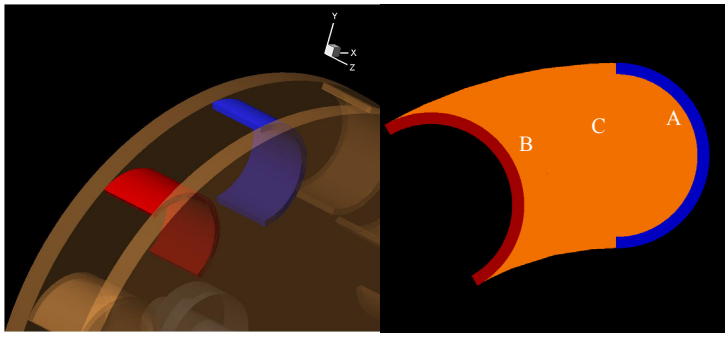

Fig. 4 Flow passage and walls

In the experiment, the runner flow is investigated under various nozzle setting conditions of the nozzle angle θ and the offset distance ΔZ. The jet and the runner in the MPS simulation are shown in Fig.3. The jet axis is set in the horizontal direction. In this study, only the flow in a single passage between adjacent two blades is simulated due to the memory capacity of our computer, although the flow discharged from the passage would affect the turbine performance by impinging the runner again as secondary effects. The jet pitch circle diameter D_1 is taken as a simulation parameter instead of the nozzle angle θ and the offset distance ΔZ used in the experiment for ease of numerical treatment, because the jet pitch circle diameter D_1 depends on the angle θ and the distance ΔZ and considered as the main parameter of the nozzle setting if we neglect the secondary effects caused by the discharged flow out of the passage. We assume that the jet has uniform velocity of V_j over its circular cross-sectional area at the nozzle outlet. Fluid particles are introduced at the grid points arranged at equal intervals of ℓ_0 on the circular cross-sectional area of the jet. Fluid particles are additionally introduced at equal intervals ℓ_0 in the flow direction to represent the continuous jet being spouted from the nozzle. As mentioned above, only the flow in a single passage between adjacent two blades is simulated. The jet portion that would enter the flow passage is defined by a geometrical approach in advance of the simulation under the assumption that the jet is cut out by the tips of the two blades without caused any velocity change and deformation, although the velocity change and the deformation of the jet portion are calculated in the simulation. As for the wall particles, as shown in Fig.4, four solid wall parts of which the flow passage consists are represented by wall particles using the method proposed by Nakanishi et al.[8,9]: A for the front side of the preceding blade, B for the back side of the following blade, C for the two endplates.

4. Experimental result

4.1. Measurement of power characteristics

The influence of the positional relation of the runner and nozzle on the runner efficiency was investigated. The nozzle offset distance shown in Fig. 1 was set equal to $\Delta Z/D_B$=0.0, 0.23, 0.45 and the nozzle angle was set equal to θ=0, 10, 20, 30°.

Figure 5 shows the runner efficiency, η, for different θ at $\Delta Z/D_B$=0. In this case, nozzle angle θ has almost no influence on the efficiency η. For any angle θ, η reaches the maximum (η_{max}) at around λ=0.55, and η_{max} is about 0.51. Figure 6 shows the runner efficiency η for different θ at $\Delta Z/D_B$=0.45. η_{max} increases with increasing θ. With large offset distance of the nozzle and small θ, in other words, with large jet pitch circle diameter D_1, a part of the water jet does not contact with the blade and directly flows out to the

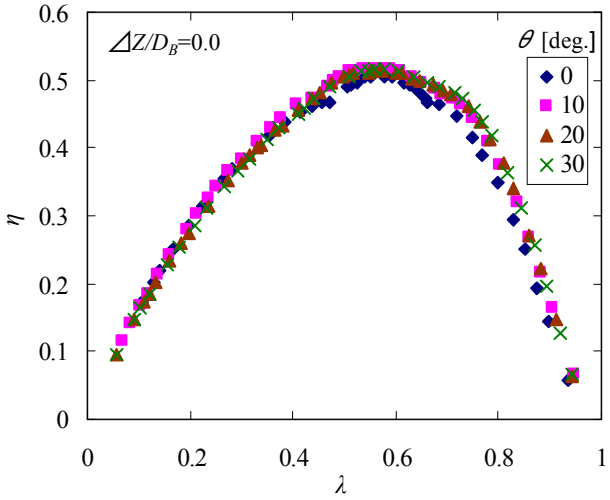

Fig. 5 Runner efficiency for $\Delta Z/D_B$=0.0

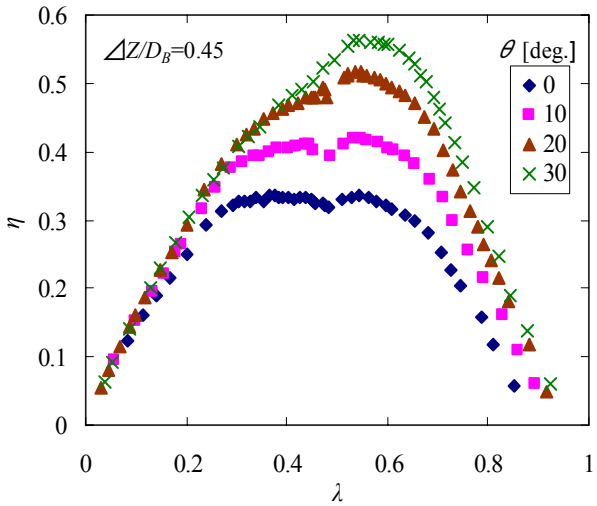

Fig. 6 Runner efficiency for $\Delta Z/D_B$=0.45

bottom of the casing. The increase of θ weakens this tendency and at θ=30° all the water jet strikes against the blade, since the increase in θ makes D_1 smaller. For $\Delta Z/D_B$ =0.45 and θ =30°, the maximum value of runner efficiency is obtained as η_{max}=0.56 among the present experimental conditions. The runner efficiency reaches the maximum value η_{max} when the tip speed ratio is λ ~0.55. In addition, discontinuity of the efficiency curves at λ ~0.5 is found. The observation of the flow around the runner clarified that this is because the water jet striking against the blade flows into the runner when λ ~0.5.

Figure 7 shows the relation between η_{max} and the nozzle setting condition. When the offset distance $\Delta Z/D_B$ = 0 and 0.23, η_{max} are approximately 0.51 and 0.55 respectively independent of nozzle angle θ. When $\Delta Z/D_B$ =0.45, on the other hand, η_{max} increases linearly with increasing θ. From the experimental results, the nozzle setting conditions for the highest runner efficiency are sets of $\Delta Z/D_B$ =0.23 and θ=0°, and of $\Delta Z/D_B$ =0.45 and θ=30°, both giving η_{max}=0.56 at 0.54<λ<0.58.

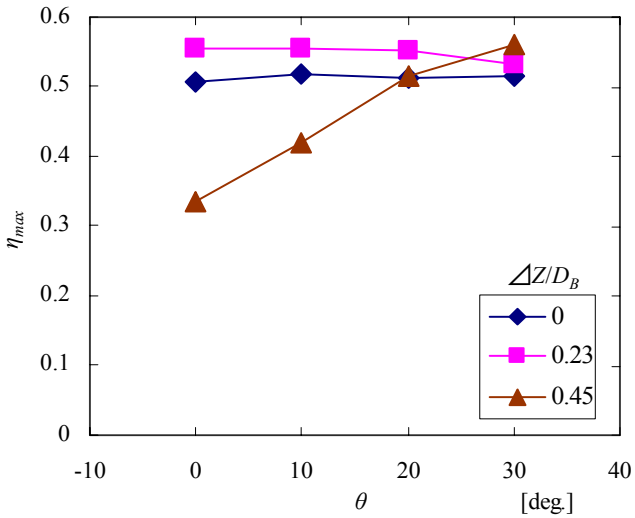

Fig. 7 Variation of η_{max} with θ and $\Delta Z/D_B$

4.2. Flow visualization

Photographic recordings of the flow visualization were obtained by employing a six-megapixel camera positioned outside the transparent casing wall opposite the runner end plate. The shutter speed was 1/8000s. The flow field was illuminated by a flashlight. A 0.31-megapixel digital video camera with a frame rate of 30 fps and a stroboscope with Xenon flash lamp were used for the video recordings.

The typical visualization results are depicted in Figs. 8 (a) to (c) at $\Delta Z/D_B$ =0, 0.23, 0.45 with nozzle angle θ=0°. In these cases, the tip speed ratio λ was set to the value that gave the maximum runner efficiency. Below each photo that visualized the entire runner, a magnified photo near the blade against which the water jet strikes is presented. The horizontal dotted-dashed lines show the central line of the water jet and the other dotted-dashed lines show the center of the blade against which the water jet strikes.

The water jet from the nozzle strikes against the blade and flows to both the inside and outside of the runner. The blade in the vertically-up direction from the runner axis and its right-hand neighbor mainly receive the water jet. The water jet strikes against the blade

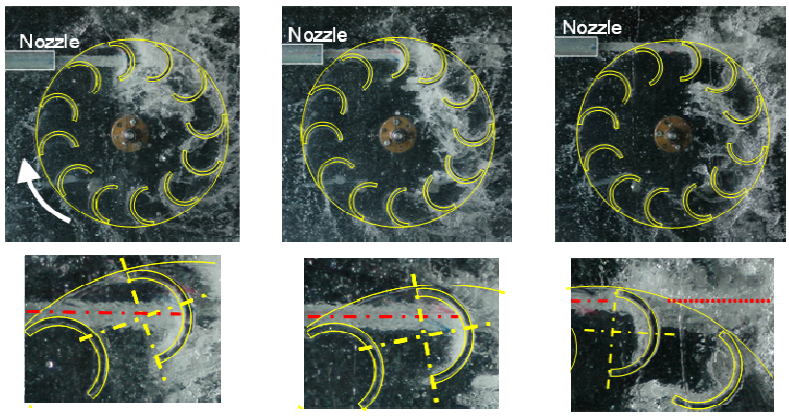

(a) $\Delta Z/D_B$=0.0 (b) $\Delta Z/D_B$=0.23 (c) $\Delta Z/D_B$=0.45

Fig. 8 Flow patterns in various nozzle setting conditions

around the center of the blade in Fig.(a). The position where the jet strikes against the blade shifts outwards with increasing $\Delta Z/D_B$ or D_1 from Fig.(a) to Fig.(c). In Fig.(c) with the largest D_1, part of the water jet does not contact the blade as shown by the red dotted line as its center line. The water jet strikes against only one blade, while under other conditions it strikes against two blades at least. This is the cause of the significant reduction of the runner efficiency.

The flow visualization also shows that the jet impinges on the back side of the blade in the final stage of the flow in the one flow passage. In this study, therefore, numerical simulation investigates the free surface flow in the runner with impingement of the jet against the back side of the blade and estimates the output power of the runner.

5. Numerical result

Numerical simulation based on MPS method was conducted to investigate the free surface flow in the runner and to estimate the output power of the runner. A conventional approach using the momentum theorem could not be applied to the flow in the runner, because the flow in the runner is unsteady and we also have to consider the impingement of the flow against the back side of the blade as observed in the experiment.

The jet pitch circle diameter D_1 was taken as a simulation parameter instead of the nozzle angle θ and the offset distance ΔZ as mentioned before and it was set to D_1= 180, 200, 220, 240mm, that corresponds to $\Delta Z/D_B$= -0.23, 0.0, 0.23, 0.45. The tip speed ratio was set to λ = 0.55.

The initial particle distance was taken as ℓ_0 = 0.55mm, or 20 particles to the length of the jet diameter. The kernel sizes were given as r_e=4.0ℓ_0 for Eq. (1) and 2.0ℓ_0 for the others according to the similar simulations[8,9] for a Pelton turbine. The Poisson equation of pressure expressed by the particle interaction model Eq. (5) was solved by ICCG (the incomplete Cholesky decomposition conjugate gradient method). The turbulence effects and the surface tension of the water were not considered. The free surface parameter and the time step were given as β=0.97 and Δt =0.5ℓ_0/V_j, respectively.

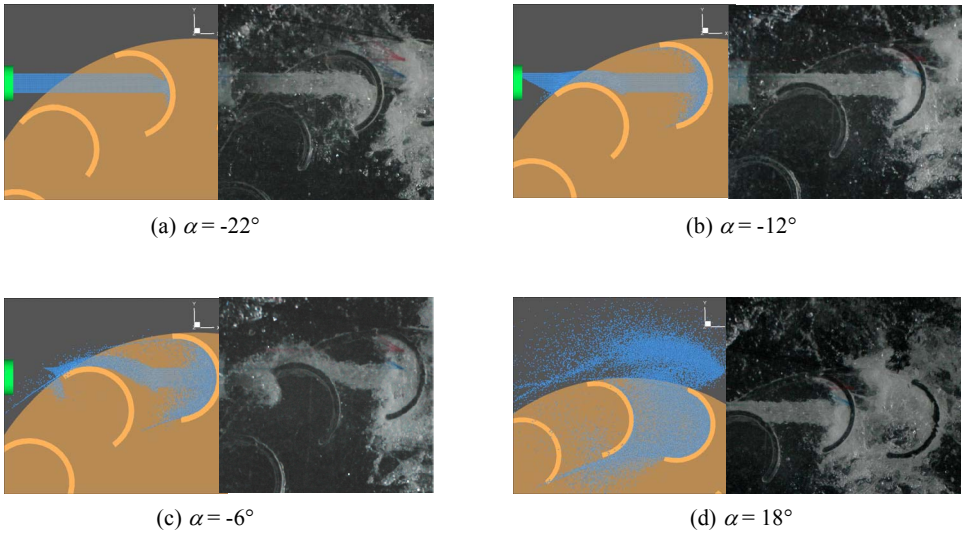

(a) α = -22° (b) α = -12°

(c) α = -6° (d) α = 18°

Fig. 9 Comparison of flow patterns

Figure 9 shows the typical examples of numerical results at D_1= 200mm ($\Delta Z/D_B$= 0.0) with the corresponding visualized results obtained by the experiment. In Fig.9, α denotes the rotation angle of the preceding blade of the flow passage under consideration, α=0 gives the blade position where the jet strikes the preceding blade perpendicularly to its chord.

Figure (a) shows the results at α = -22°. This is the instant of first contact of the jet with the preceding blade. The head shape of the jet given in the simulation is consistent with the experimental result, although the shape of the jet was defined by the geometrical approach that the jet was cut out by the tips of the blades. In Fig.(b) at α = -12°, we can see that the jet begins to spread on the preceding blade and the rear part of the jet contacts the back side of the following blade. In Fig.(c) at α = -6°, the rear part of the jet is lifted up by the following blade. The deformation of the jet is well predicted by this simulation. In Fig.(d) at α = 18°, we can see the swashed water out of the runner. It seems that the fluid particles observed inside the blades is less than that in the experiment. It is because this simulation analyzed one flow passage between adjacent two blades. The water we can see under the preceding blade in the experimental results is the discharged one from other flow passages.

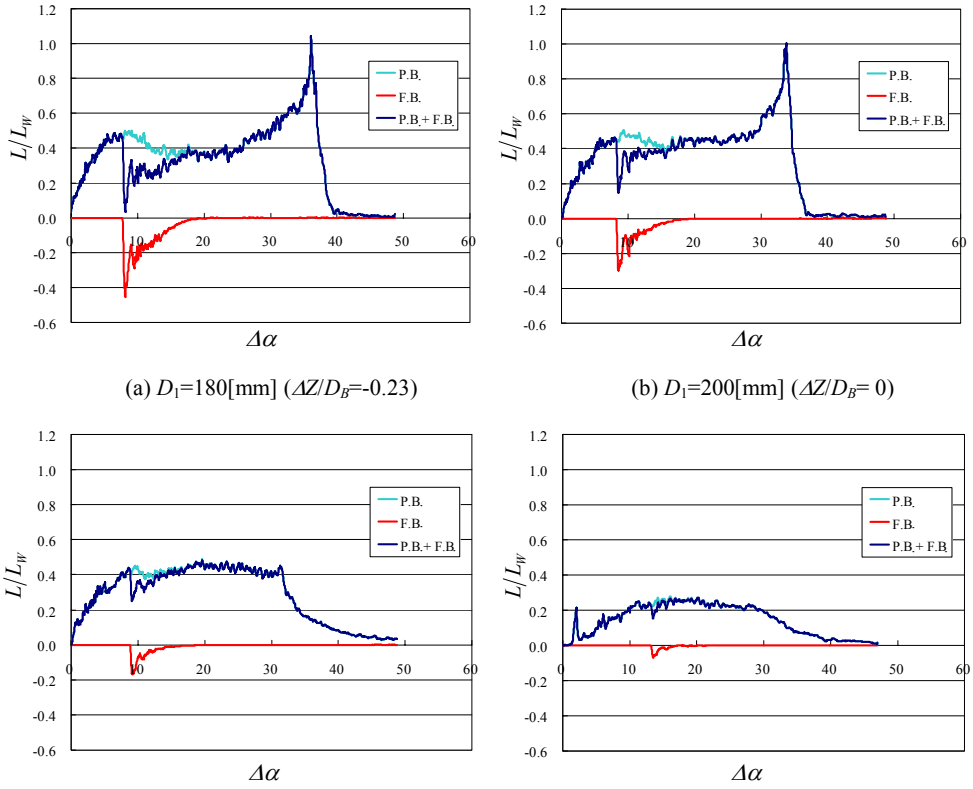

(a) D_1=180[mm] ($\Delta Z/D_B$=-0.23)

(b) D_1=200[mm] ($\Delta Z/D_B$= 0)

(c) D_1=220[mm] ($\Delta Z/D_B$= 0.23)

(d) D_1=240[mm] ($\Delta Z/D_B$= 0.45)

Fig.10 Output powers of preceding and following blades

The contact of the rear part of the jet with the back side of the following blade was observed both in the experiment and in the simulation. The effect of the jet contact on the output power was checked from the results of the numerical simulation. The output power L generated by the front side of the preceding blade (P.B.) and by the back side of the following blade (F.B.) is shown in Fig. 10. $\Delta\alpha$ denotes the rotation angle of the preceding blade after the first contact of the jet with the blade. Figure (a) shows the output power at D_1=180mm ($\Delta Z/D_B$= -0.23). The output power by the preceding blade becomes larger as $\Delta\alpha$ increases. On the other hand, the negative power by the following blade reaches the peak when the rear part of the jet touches the back side of the blade and then goes down gradually. The output power at D_1=200mm ($\Delta Z/D_B$= 0) as shown in Fig.(b) has a tendency similar to that at 180mm ($\Delta Z/D_B$= -0.23). Different from Figs. (a) and (b), the output powers of the preceding blade at D_1=220mm ($\Delta Z/D_B$= 0.23) and D_1=240mm ($\Delta Z/D_B$= 0.45) do not increase as $\Delta\alpha$ increases as shown in Figs (c) and (d) because the rear part of the jet lifted

up by the following blade almost never enters the preceding blade due to its large jet pitch circle diameter D_1, although the output power by the following blade decreases with increasing D_1. These results demonstrate that the effect of the jet impingement against the back side of the blade is significant to evaluate the runner performance if we use this simple shape of runner.

The runner efficiency η was estimated from numerical results under the assumption that each flow passage of the runner has equal contribution to the output power of the runner when it receives the jet. The runner efficiency estimated by numerical simulation is compared with that measured in the experiment as shown in Fig.11. The runner efficiency obtained in the experiment was plotted in terms of the corresponding jet pitch circle diameter D_1. The Figure 11 shows that the numerical simulation well predicts the tendency of the runner efficiency to the jet pitch circle diameter D_1.

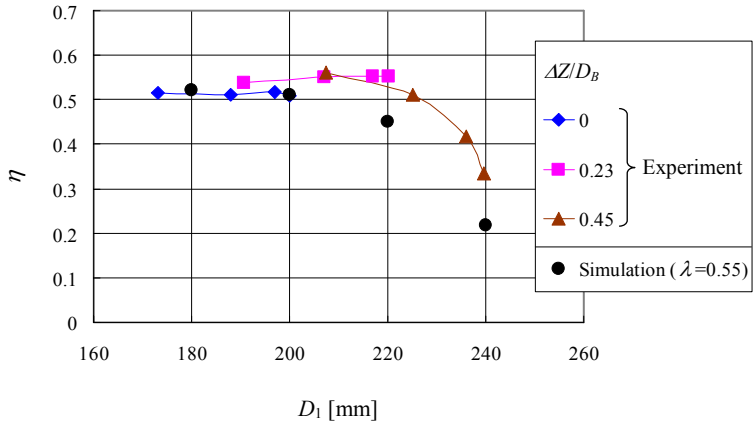

Fig.11 Comparison of runner efficiency

6. Conclusions

To develop a hydraulic turbine to utilize unexploited water resources as nano hydropower, we proposed a newly-designed impulse turbine with the simplest components of the minimum requirements. As a first step of the study, the flow in the runner and the output power were investigated experimentally and numerically to acquire a guideline for future practical applications. The maximum runner efficiency of 0.56 is obtained in the experiment. The experimental and numerical results reveal that the nozzle setting conditions is one of the important factors to realize high efficiency of runner. The numerical simulation shows that the impingement of the jet against the back side of the blade is significant for the flow in the runner and the efficiency.

In order to improve this turbine, it is necessary to examine the setting angle of the blade in the runner, the number of the blades, the size and shape of the blade as well as the nozzle position in this paper. In addition to the experimental approach, the numerical simulation based on the MPS method will be helpful tool to analyze the free surface flow in this kind of impulse turbine and its efficiency. Further experimental and numerical investigations may enable us to develop impulse-type simple turbines for nano hydropower.

Acknowledgement

The work was partially supported by a Grant-in-Aid for Exploratory Research (No.19651033) from the Japanese Ministry of Education, Culture, Sport, Science and Technology for which the authors wish to express their sincere gratitude.

References

(1) Riaz, R. A., Ail, N., The development of small hydro for remote areas of northern Pakistan, *International Water Power & Dam Construction*, Vol.43, No.5(1991), pp.24-26.

(2) Williams, A., Pico practice, *International Water Power & Dam Construction*, Vol.56, No.3 (2004), pp.24-25.

(3) Nishimura, M., Yamato, S., Takahashi, M., Micro Hydropower for Mountaineering Cottage, *Turbomachinery*, Vol.30, No.3 (2002), pp.155-160.

(4) Nemoto, M., Akaike, S., Mori, T., Electric Power Generation by Micro-Hydroturbine at Mountain Hut, *Turbomachinery*, Vol.30, No.4 (2002), pp.193-200.

(5) D. Agar, M. Rasi, On the use of a laboratory-scale Pelton wheel water turbine in renewable energy education, *Renewable Energy*, In Press, Corrected Proof, Available online 23 October 2007.

(6) Kikuchi, R., Nakamichi, S., Nakamura, M., Kaga, T., Matsuzaki, H., Takahashi, S., The Design and Expriment of a Water Turbine Generator with Nano Class Capacity, *The bulletin of Hachinohe Institute of Technology*, Vol.24 (2005), pp.9-18.

(7) Koshizuka, S. and Oka, Y., Moving-Particle Semi-Implicit Method for Fragmentation of Incompressible Fluid, *Nuclear Science and Engineering*, Vol.123 (1996), 421-434.

(8) Nakanishi, Y. and Fujii, T., Numerical Simulation of the Flow in a Pelton Bucket by a Particle Method (1st Report, Flow in a Rotating Bucket using Relative Jet Paths), *Transactions of the Japan Society of Mechanical Engineers*, *Series B*, Vol.73, No.728 (2007), pp. 1008-1013.

(9) Nakanishi, Y., Fujii, T. and Wachi, K., Numerical Simulation of the Flow in a Pelton Bucket by a Particle Method (2nd Report, Flow and Output Power of Runner at Off-design Operating Points), *Transactions of the Japan Society of Mechanical Engineers*, *Series B*, Vol.73, No.736 (2007), pp. 2524-2529.